Lattice dynamics and the diffuse phase transition of lithium sulphide investigated by coherent neutron scattering

1991 J. Phys.: Condens. Matter 3 1055

(http://iopscience.iop.org/0953-8984/3/9/002)

J. Phys.: Condens. Matter 3 (1991) 1055–1064. Printed in the UK

Lattice dynamics and the diffuse phase transition of lithium sulphide investigated by coherent neutron scattering

W Buehrer†, F Altorfer†, J Mesot†, H Bill‡, P Carron‡ and H G Smith§

† Labor für Neutronenstreuung, ETHZ, CH-5232 Villigen PSI, Switzerland

‡ Departement de Chimie physique, Sciences II, Quai E Ansermet 30, CH-1211 Genève 4, Switzerland

§ Solid State Division, Oak Ridge National Laboratories, Oak Ridge, TN 37830, USA

Received 28 September 1990

Abstract. Elastic neutron diffraction of Li_2S, measured as a function of temperature, shows the onset of a diffuse phase transition near 900 K to a highly conducting state. Inelastic neutron scattering has been used to investigate the harmonic lattice dynamics of Li_2S at 15 K. A shell model has been successfully fitted to the data. The dynamical properties are computed within the harmonic approximation and compared with experimental data.

1. Introduction

Lithium sulphide (Li_2S) crystallizes in a face-centred cubic lattice with one formula unit per primitive cell. The space group is O_h^5 ($Fm3m$), and the structure is anti-morphous to the fluorites. In recent years, fluorites and anti-fluorites have attracted attention owing to their high-temperature properties, i.e. a diffuse ('Faraday') transition to a highly ionic conducting phase at temperatures $T_F = (0.6\text{–}0.8)T_{melt}$ (for a review on fluorites see Hayes (1986)). The materials are therefore referred to as superionic conductors. They find technological applications in batteries (as solid electrolytes and/or as ion insertion compounds), in fuel cells or in solid state gas detectors.

The sulphur-based anti-fluorites are relatively unexplored. Recent electrical conductivity measurements on single crystals (Carron 1990) showed a high ionic conductivity for Li_2S ($\sigma = 0.15\ \Omega^{-1}\,cm^{-1}$ at 1000 K); furthermore, in a 'standard plot' of $\ln(\sigma T)$ versus $1/T$, a change in slope occurs near 800 K which might be associated with the onset of a diffuse transition. The melting point of Li_2S is 1645 K, and the ratio T_F/T_{melt} is about 0.5. This value is near the 'best' observed for fluorites (PbF_2), with a wide range between T_F and T_{melt}. Unfortunately, there exists no measurement of the specific heat of Li_2S which would give more direct evidence of the transition.

In the present paper we report, in addition to a lattice dynamics study (see below), the observation of a diffuse transition by elastic neutron scattering of a polycrystalline sample. The transition temperature (about 900 K), derived from site occupancies, is in fair agreement with the ionic conductivity experiments.

The high conductivity is assumed to be a consequence of Frenkel defect generation. The creation of defects is closely related to the thermal motion of the ions, and therefore knowledge of the ion dynamics is crucial for the understanding of the mechanism of ionic conductivity in superionic conductors. The instantaneous position of the conducting ion

0953-8984/91/091055 + 10 $03.50

relative to its neighbours is of central interest in the diffusion process and represents a suitable reaction coordinate for ionic jumps which can be represented in terms of the phonon structure (frequencies, eigenvectors and density of states (Flynn 1972)).

A lattice dynamical study was therefore initiated using coherent inelastic neutron scattering of a single crystal, performed at 15 K in order to characterize the system in the 'harmonic' state. The subsequent calculation with a shell model successfully describes the dispersion curves. An anharmonic extension of the model could be used to estimate theoretically the defect formation energies and to provide the basis for computer simulations of possible high-temperature structures and of the dynamics of ions in the disordered state.

2. Experiment

Lithium in its natural isotopic composition has a rather high absorption cross section for thermal neutrons. Therefore ^{7}Li-enriched material was used. The details of the sample preparation as well as the single-crystal growth have been described by Carron (1990). The crystal was of cylindrical shape with [001] axis, the volume was about 2.5 cm^3, and the mosaic spread was better than 0.4°. Li_2S is very hygroscopic and therefore all the samples were handled in a glove-box in a dry helium or argon atmosphere. The neutron scattering experiments were performed at the reactor Saphir in Würenlingen. The inelastic measurements were conducted on the triple-axis spectrometer; the monochromator and analyser were pyrolitic graphite, and the monochromator was used in its doubly focusing mode of operation. Normal constant-Q and constant-ω techniques with fixed analyser energy were applied. In order to overcome anharmonic effects, common to all fluorites, the crystal was mounted in a closed-cycle refrigerator and the experiment was performed at 15 K. The elastic experiments on $^7Li_2S$ powder were conducted on the multi-detector spectrometer DMC with an incoming wavelength of 1.706 Å. The sample was contained in a thin-walled vanadium can, and data were collected in the temperature range 10 K $< T <$ 1320 K with a closed-cycle refrigerator or vacuum furnace, respectively.

3. Crystal structure and phase transition

Neutron diffraction patterns of $^7Li_2S$ powder were measured at 10, 295, 670, 920, 1020 and 1320 K. Two characteristic diagrams are shown in figure 1 (10 and 1320 K); because of the negative scattering length of Li the intensities are different from the 'standard fluorite' pattern. The diagrams show some weak foreign lines (due to polysulphides, lithium ethanolate and the thermocouple). The pattern of main lines does not change as a function of temperature, i.e. there is neither an enlargement of the unit cell nor a change in symmetry. The pairwise comparison of intensities (e.g. (111)–(200); (311)–(222)) for the two temperatures (figure 1) shows a relative decrease in the 'strong' even lines which can be associated with increasing disorder in the lattice. This diffuse transition shows up more clearly by looking at the intensity of the (111) peak, plotted as a function of temperature (figure 2). In the perfect Li_2S lattice, structure factors can be grouped into three classes (neglecting the Debye–Waller factors):

'strong'	$F = b_S - 2b_{Li}$	h, k, l even	$h + k + l = 4n + 2$
'medium'	$F = b_S$	h, k, l odd	
'weak'	$F = b_S + 2b_{Li}$	h, k, l even	$h + k + l = 4n$

where the scattering lengths are $b_S = 0.285 \times 10^{-12}$ cm and $b_{^7Li} = -0.22 \times 10^{-12}$ cm (Koester *et al* 1981).

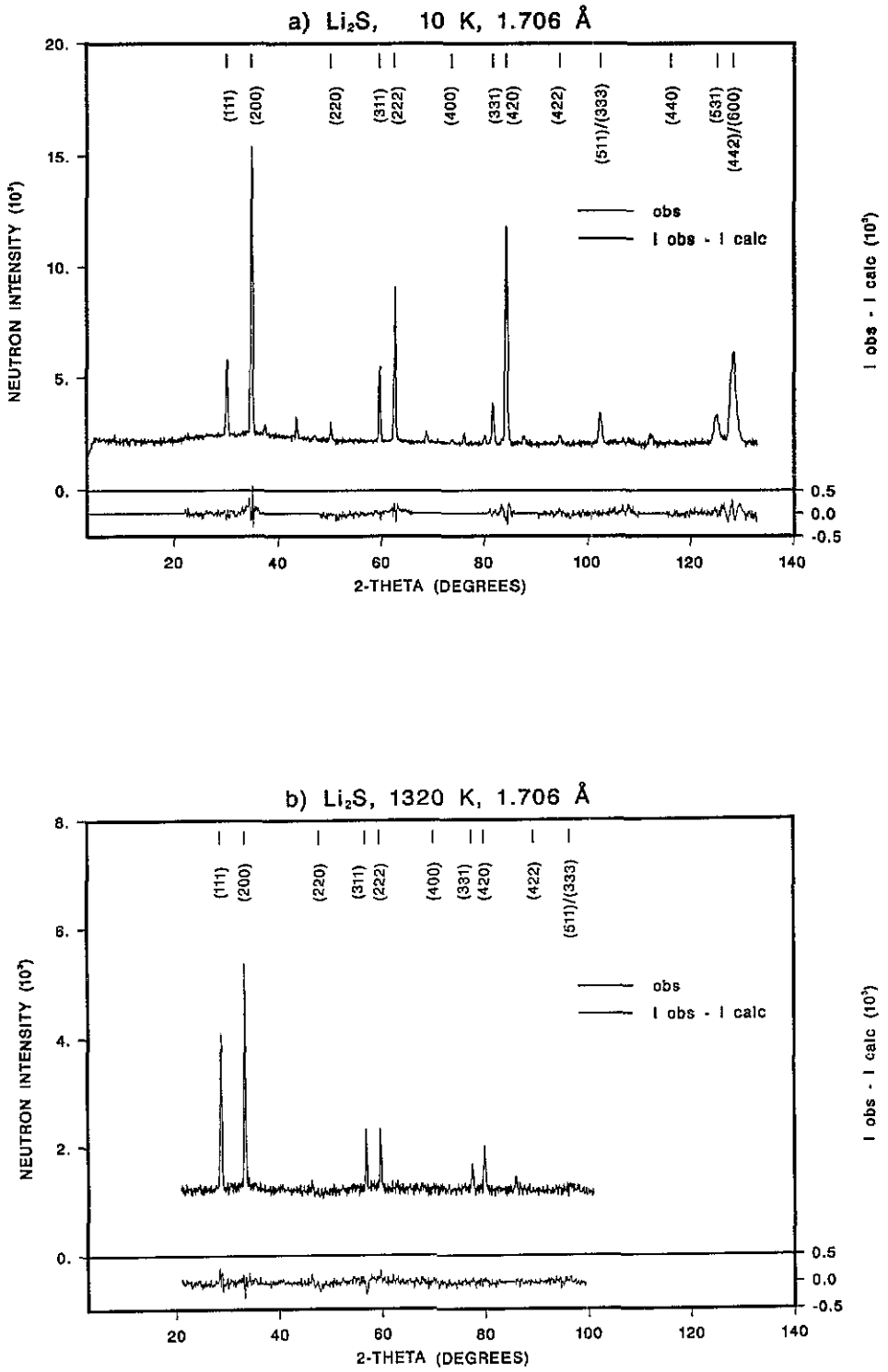

Figure 1. Neutron diffractograms of $^7Li_2S$; experimental and difference diagrams (λ = 1.706 Å): (*a*) 10 K; (*b*) 1320 K.

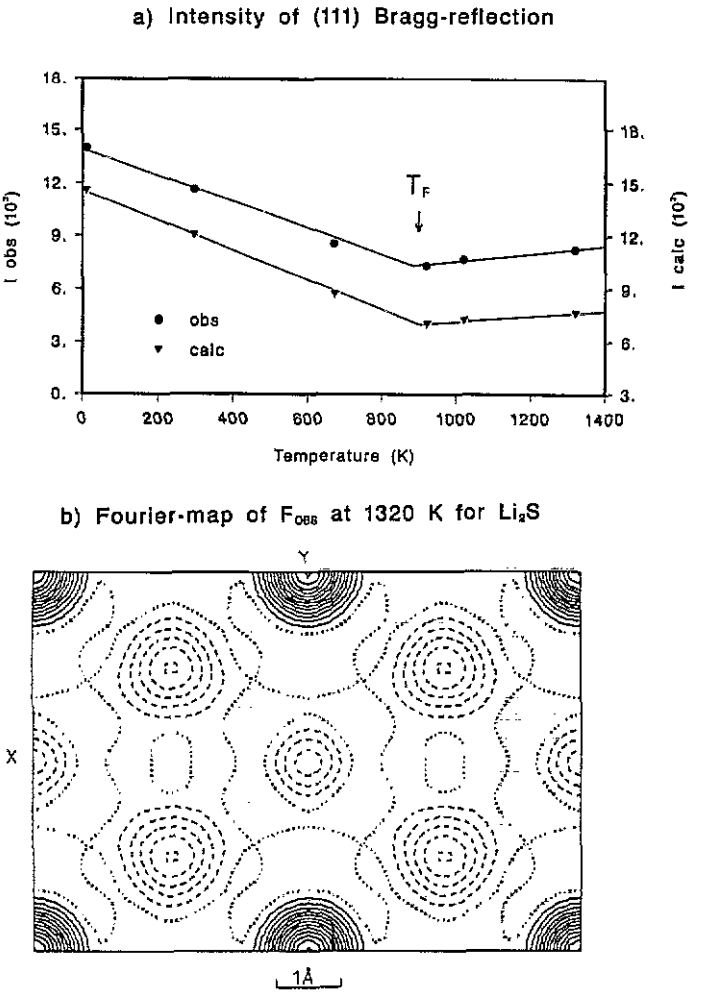

Figure 2. (*a*) Neutron intensity of elastic (111) reflection of $^7Li_2S$ as a function of temperature: the lines are a guide to the eye; T_F marks the onset of the diffuse transition. (*b*) Fourier map of F(obs) at 1320 K for Li_2S where contour lines correspond to 0.2 of the minimum (– – –): · · · · ·, zero line. x is parallel to [100], and y parallel to [00$\bar{1}$].

For h, k, l odd, only sulphur contributes to the structure factor; therefore the observed intensity increase with increasing temperature (figure 2) can only be explained with the occupation (in the time average) of new 'non-perfect' fluorite sites by lithium ions. From the figure, we estimate the transition temperature T_F to be near 900 K.

For the quantitative analysis the data have been refined with the program of Wiles and Young (1982). The peak shape was assumed to be Gaussian, and the background was represented by a self-adjusting polynomial. The results are summarized in table 1. For temperatures $10\text{K} \leqslant T \leqslant 670$ K, a good R-factor could be obtained with the regular crystal structure and isotropic harmonic Debye–Waller factors. For higher temperatures, defects had to be taken into account. A satisfactory agreement was obtained with the simple Frenkel defect, i.e. by allowing the Li ions to leave the regular sites and to occupy the centres of the empty cubes ($\frac{1}{2}$, $\frac{1}{2}$, $\frac{1}{2}$ sites). A 14% occupation at 1320 K for

Table 1. $^7Li_2S$; structural parameters as a function of the temperature. Profile refinement according to Wiles and Young (1982). (Space group, $Fm3m$ (O_h^5); sulphur ions on positions 4a; lithium on positions 8c and, above 800 K, partially on 4b.)

Temperature (K)	a (Å)	$n_{Li(8c)}$	$n_{Li(4b)}$	B_S (Å^2)	B_{Li} (Å^2)	R_{exp}	R_{wp}
10	5.689	1.000	—	0.21(4)	0.59(4)	1.97	3.00
295	5.722	1.000	—	0.43(7)	0.54(7)	3.04	4.06
670	5.760	1.000	—	1.66(7)	2.43(7)	2.03	3.04
920	5.859	0.988(5)	0.012(5)	3.0(2)	5.5(2)	2.18	3.79
1020	5.885	0.973(5)	0.027(5)	3.8(2)	7.4(3)	1.71	3.31
1320	5.944	0.864(6)	0.136(6)	5.5(3)	8.8(6)	2.78	4.34

these sites looks quite reasonable; this value is rather well determined because it is mainly derived from the observed intensity increase of the 'medium' lines, and not from the decrease in the intensity of the 'strong' lines. Therefore the occupational parameter is anti-correlated with the Debye–Waller factor which gives an overall intensity decrease, a behaviour that parallels a 'spread' of ions throughout the unit cell. The difference diagrams for 10 and 1320 K are plotted in figure 1 (bottom); the straight lines mark regions excluded in the fit. The calculated intensities of the (111) peak are shown in figure 2; the intensity increase above about 900 K is well reproduced. A Fourier map at 1320 K, based on F(obs), is plotted in figure 2(b). The section through the (110) plane clearly shows additional intensity at $(\frac{1}{2}, \frac{1}{2}, \frac{1}{2})$ sites. More complicated models, as introduced by Dickens *et al* (1982) for PbF_2, did not improve the quality of the fit.

4. Lattice dynamics at 15 K

Figure 3 shows the measured phonon dispersion curves of Li_2S along the symmetry directions Δ, Σ, Λ and Z; the group theoretical notation is according to Warren and Worlton (1973). In order to observe and separate the different branches, the crystal was aligned with orientations $[1\bar{1}0]$, [001] and $[11\bar{6}]$. Experimental errors are about 2% and 5% for the low- and high-energy modes, respectively. The zone-centre Raman-active mode ('breathing' type of motion of the two Li ions) agrees well with the optical data (Carron 1990), its frequency is higher than that of the infrared-active mode (transverse optic (TO)). It is interesting to note that this sequence is changed in the isostructural compounds Na_2S (Buehrer and Bill 1980) and Li_2O (Farley *et al* 1988); for Na_2S (with a heavier mass of the cation) this behaviour can be expected, but for Li_2O this is rather strange; in addition, Li_2O shows a much larger TO–LO splitting than Li_2S does. In other words, the 'chemically expected' relationship between Li_2S and Li_2O is not reflected in the inter-ionic bonding properties.

A comparison 'by eye' of the overall features of fluorite dispersion curves shows a striking similarity between $^7Li_2S$ and CaF_2 (Elcombe and Pryor 1970) with respect to the range of frequencies, mode sequence (infrared, Raman) in the zone centre, and TO–LO splitting.

The experimental frequencies have been analysed with different models for the lattice dynamics within the harmonic, adiabatic and electrostatic approximations; Elcombe and Pryor (1970) have given full details. The parameters of the models were determined by a least-squares refinement, minimizing the χ^2-function. Phonons from

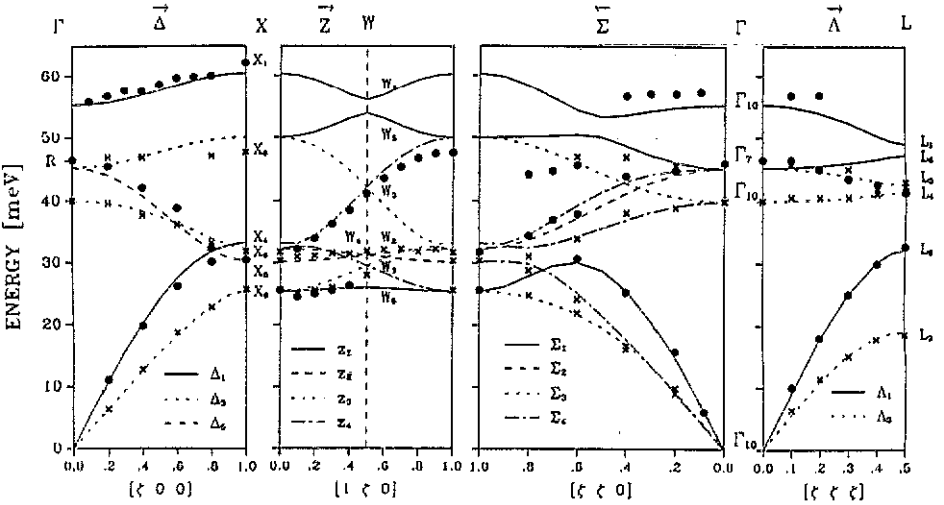

Figure 3. Phonon dispersion of $^7Li_2S$ at 15 K where the polarizations (●, longitudinal; ×, transverse) are determined by the experiment: ——, best-fit shell model calculation (parameters in table 2). The wavevector ζ is in units of $2\pi/a$. The group theoretical notation is according to Warren and Worlton (1973).

all symmetry directions have been used in the fit. During the minimization procedure, in each iteration, the calculated frequencies were grouped according to their symmetry (by block diagonalization of the dynamical matrix) in order to compare them with the corresponding experimental points.

The short-range potential is represented by the parameters A_{ij} and B_{ij} for the pairwise interaction of Li–S, Li(1)–Li(2) (different sublattices), S–S and Li–Li (same sublattice). The rigid-ion model does not reproduce the experimental frequencies very well; however, parameters are included in table 2 since, for molecular dynamical simulations, one often prefers a simple model, tractable on the computer. Good agreement is obtained with the shell model, with both types of ion polarizable. The calculated dispersion curves are displayed in figure 3; the best-fit values of the 13 parameters are given in table 2, together with the shell charges and the shell–core spring constant.

Derived quantities from the model are also given in table 2. The high-frequency dielectric constant is rather small, showing a tendency to covalent bonding in Li_2S. The elastic constants have been determined from the initial slopes of the measured dispersion curves with a residuum calculation, taking into account all seven acoustic modes in the high-symmetry directions. The corresponding values derived from the shell model agree surprisingly well in view of the fact that the fitting process mainly optimizes the higher-energy phonon modes; in fact the shell model reproduces the phonon frequencies for all wavevectors quite well.

The frequency distribution function $g(\omega)$ for the normal modes of vibration of Li_2S has been computed from the model shown in table 2. We used the extrapolation method (Gilat and Raubenheimer 1966) to sample the frequencies at a large number of wavevectors. The density of states is shown in figure 4(*a*). An interesting insight into the dynamics of a system is offered by means of the displacement–displacement correlation functions (Maradudin *et al* 1971) which are obtained by weighting the density of states with the eigenvectors of the different ions; the result is shown in figure 4(*b*). The energy separation between the two ionic species close to 32 meV is remarkably clear; sulphur

Table 2. $^7Li_2S$ at 15 K: least-squares model parameters and derived quantities (details of the models given by Elcombe and Pryor 1970): *e is the electronic charge, and v is the volume of* the primitive unit cell.

Parameter		Units	Rigid-ion model	Shell model	Experiment[a]	
A_1	Li–S	e^2/v	5.100	5,377		
B_1	Li–S	e^2/v	0.424	0.411		
A_2	Li(1)–Li(2)	e^2/v	1.232	1.233		
B_2	Li(1)–Li(2)	e^2/v	−0.266	−0.266		
A_3	S–S	e^2/v	1.129	1.118		
B_3	S–S	e^2/v	−0.202	−0.182		
A_4	Li_1–Li_1	e^2/v	0.199	0.177		
B_4	Li_1–Li_1	e^2/v	0.004	0.022		
Z	S	e	0.970	1.000		
α	Li	Å^3	—	0.044		
d	Li	e	—	−0.007		
α	S	Å^3	—	1.046		
d	S	e	—	−0.049		
χ^2			6.6	4.7		
			Shell properties			
Y	Li	e	—	1.21		
k	Li	e^2/v	—	1527		
Y	S	e	—	7.65		
k	S	e^2/v	—	2571		
			Derived quantities			
ε_∞			1.0	1.35		
c_{11}		10^{11} dyn cm^{-2}	9.23	9.46	9.54	0.35
c_{12}		10^{11} dyn cm^{-2}	2.41	2.17	2.09	0.23
c_{44}		10^{11} dyn cm^{-2}	3.12	3.23	3.19	0.08

[a] *Fit to small-wavevector acoustic phonons.*

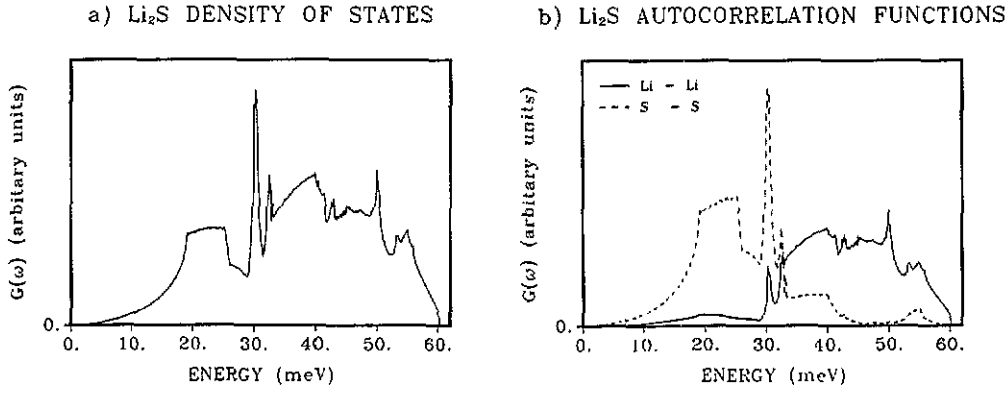

Figure 4. *(a)* Frequency distribution $g(\omega)$ *for phonons in* $^7Li_2S$, *calculated with the shell* model; *(b)* eigenvector-weighted densities of states for Li and S in $^7Li_2S$, calculated with the shell model.

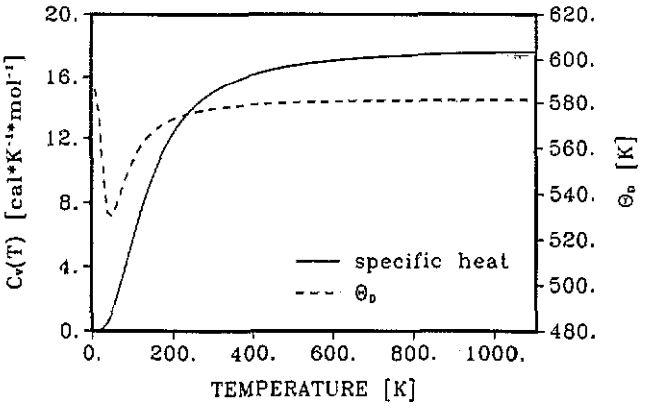

Figure 5. Specific heat $C_V(T)$ and related Debye temperature $\Theta_D(T)$ for $^7Li_2S$, computed with the shell model in the harmonic approximation.

moves predominantly in the lower-frequency modes, whereas lithium is mainly involved in the higher optic modes. Dynamical quantities may readily be computed within the harmonic approximation (Maradudin *et al* 1971). The temperature dependence of the specific heat C_V is shown in figure 5, together with the corresponding Debye temperature $\Theta_D(T)$. No experimental values have been found in the literature for direct comparison. The calculated mean square ionic displacements for the individual ions are shown in figure 6. The comparison with the values from the diffraction experiments shows, for both ionic species, good agreement up to temperatures near the diffuse transition.

5. Discussion

The low-temperature dynamics of Li_2S can be successfully described by the shell model, a model originally developed for ionic solids (Cowley *et al* 1963). This is in a way surprising because the high melting temperature of Li_2S suggests some covalent character in the atomic bonding; furthermore sulphur has a rather complex electronic polarizability (e.g. formation of polysulphides) which might influence the phonon dispersion curves. It turns out that the shell model is 'flexible'. It allows us to account for different types of bonding. Although the use of the shell model implies that some individual physical parameters are not uniquely defined, e.g. the ionic charge and the mechanical and electronical polarizabilities (or shell charges and core–shell force constants), the accurate determination of the dispersion curves within the model enables a good description of the harmonic crystal properties to be given. At higher temperatures, strong shifts of frequencies are observed for Li_2S by Raman scattering (Carron 1990) and by Brillouin techniques (Comins 1990). In order to treat the anharmonic lattice dynamics a parametrization of the electronic degrees of freedom as proposed by Fischer (1974) for AgCl might be more adequate.

In fluorites, the high-temperature disorder has been interpreted in terms of a model of dynamic clusters of Frenkel defects, vacancies and relaxed anions (Hutchings *et al* 1984). The present data set suggests that in Li_2S the simple defect structure, the occupation of $(\frac{1}{2}, \frac{1}{2}, \frac{1}{2})$ sites, is created. The concentration of defects is in between those observed for $SrCl_2$ and PbF_2 (Dickens *et al* 1979). By comparing the radii of ions in the fluorites with those in sulphur-based anti-fluorites, a different behaviour seems

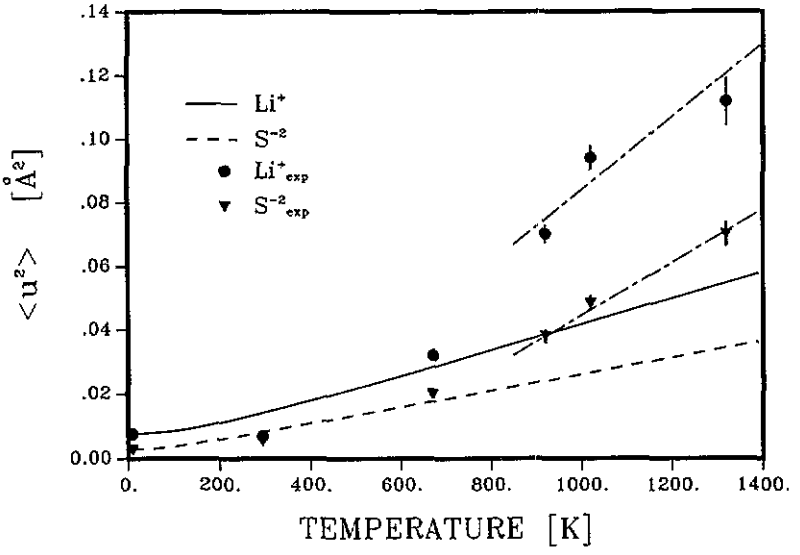

Figure 6. Mean square ionic displacements for $^7Li^+$ (——) and S^{2+} (– – –) in $^7Li_2S$, derived from figure 4(*b*); ●, ▼, *experimental values from the diffraction experiments (table 1)*; ———, guide to the eye.

plausible. In the fluorites (CaF_2, $SrCl_2$ and PbF_2), on the one hand, the mobile anions are larger than the cations which are believed to stay on the regular sites; in Li_2S, on the other hand, the resident S^{2-} anions are much larger than the Li^+ cations and form a nearly close-packed lattice. The small mobile Li^+ cations can be placed in the pockets of the sulphur sublattice, on the regular sites as well as on the interstitial sites, without an appreciable distortion of the 'scaffold structure'.

In our present picture, the Li ions diffuse along directions [*xxx*] into the empty cubes. Having a look into the lattice dynamics and searching for modes which give rise to large lithium displacements (relative to the sulphur), we have to consider zone-boundary modes with low frequencies (easy thermal activation). Modes of the 'Li-only' type (by symmetry) are at X_8, W_2, W_4 and L_4 (figure 3), and the attempt frequency for thermal activated jumps is then about 35 meV. This average frequency is derived from the 15 K data and will certainly be lower at higher temperatures.

The mean square displacements of the ions (derived from the diffraction experiment) show, within the present analysis with only one parameter for the thermal motion, a clear change in slope near the transition temperature T_F (figure 6), and the deviation from the harmonic value increases with increasing temperature. The extent of the contributions from different possible origins of this deviation, i.e. anharmonicity, anisotropy (tetrahedral) or 'quasi-static' displacements cannot be determined from the present experiments. Additional work on Li_2S in order to determine the time dependence of the diffusion process is certainly necessary.

Acknowledgments

The expert technical assistance given by the electronics and workshop groups of the Laboratory for Neutron Scattering as well as by the Saphir reactor department of

the Paul Scherrer Institute is gratefully acknowledged. A Gerber contributed to the preparation of the powder and the growth of the single crystals. The underlying work was in part supported by the Swiss National Foundation (grant 2000-005541).

References

Buehrer W and Bill H 1980 *J. Phys. C: Solid State Phys.* **13** 5495
Carron P L 1990 *Thesis* Departement de Chimie Physique, University of Geneva
Comins D 1990 private communication, University of the Witwatersrand
Cowley R A, Cochran W, Brockhouse B N and Woods A D B 1963 *Phys. Rev.* **131** 1030
Dickens M H, Hayes W, Hutchings M T and Smith C 1982 *J. Phys. C: Solid State Phys.* **15** 4043
Dickens M H, Hayes W, Smith C and Hutchings M T 1979 *Fast Ion Transport in Solids* ed P Vashishta *et al* (Amsterdam: North-Holland) p 225
Elcombe M M and Pryor A W 1970 *J. Phys. C: Solid State Phys.* **3** 492
Farley T W D, Hayes W, Hull A, Hutchings M T, Ward R and Alba M 1988 *Solid State Ionics 87* ed W Weppner and H Schulz (Amsterdam: North-Holland) p 189
Fischer K 1974 *Phys. Status Solidi* b **66** 295
Flynn C P 1972 *Point Defects and Diffusion* (Oxford: Clarendon)
Gilat G and Raubenheimer L 1966 *Phys. Rev.* **144** 390
Hayes W 1986 *Contemp. Phys.* **27** 519
Hutchings M T, Clausen K, Dickens M H, Hayes W, Kjems J K, Schnabel P G and Smith C 1984 *J. Phys. C: Solid State Phys.* **17** 3903
Koester L, Rauch H, Herkens M and Schroeder K 1981 *Juel-Report* 1755
Maradudin A A, Montroll E W, Weiss G H and Ipatova I P 1971 *Solid State Phys.* Suppl. 3 (New York: Academic)
Warren J L and Worlton T G 1973 *Argonne National Laboratory Report* 8053
Wiles D B and Young R A 1982 *J. Appl. Crystallogr.* **15** 430